Evolution of Dust in Primordial Supernova Remnants and Its Influence on the Elemental Composition of Hyper-Metal-Poor Stars

Takaya Nozawa[*], Takashi Kozasa[*], Asao Habe[*], Eli Dwek[†], Hideyuki Umeda[**], Nozomu Tominaga[**], Keiichi Maeda[‡,§] and Ken'ichi Nomoto[**,‡]

[*]*Department of Cosmosciences, Graduate School of Science, Hokkaido University, Sapporo 060-0810, Japan*
[†]*Laboratory for Astronomy and Solar Physics, NASA Goddard Space Flight Center, Greenbelt, MD 20771*
[**]*Department of Astronomy, School of Science, University of Tokyo, Bunkyo-ku, Tokyo 113-0033, Japan*
[‡]*Institute for the Physics and Mathematics of the Universe, University of Tokyo, Kashiwa, Chiba 277-8568, Japan*
[§]*Max-Planck-Institut für Astrophysik, Karl-Schwarzschild Strasse 1, 85741 Garching, Germany*

Abstract.
The calculations for the evolution of dust within Population III supernova remnants (SNRs) are presented, based on the models of dust formed in the unmixed ejecta of Type II SNe. We show that once dust grains collide with the reverse shock penetrating into the ejecta, their fates strongly depend on the initial radius $a_{\rm ini}$. For SNRs expanding into the interstellar medium (ISM) with $n_{\rm H,0} = 1$ cm^{-3}, grains of $a_{\rm ini} < 0.05$ μm are trapped in the hot gas to be completely destroyed; grains of $a_{\rm ini} = 0.05$–0.2 μm are piled up in the dense shell formed behind the forward shock; grains of $a_{\rm ini} > 0.2$ μm are injected into the ISM without being eroded significantly. The total mass of surviving dust is 0.01 to 0.8 $M_\odot$ for $n_{\rm H,0} = 10$ to 0.1 cm^{-3}. We also investigate the influence of the piled-up dust on the elemental abundances of the second-generation stars formed in the dense shell of Population III SNRs. The comparison of the calculated elemental abundances with those observed in hyper-metal-poor (HMP) and ultra-metal-poor (UMP) stars indicates that the transport of dust separated from metal-rich gas can be an important process in determining the abundance patterns of Mg and Si in HMP and UMP stars.

Keywords: dust; extinction, early universe, supernovae: general, stars; abundances, Population III
PACS: 95.30.Lz, 95.30.Wi, 97.10.Tk, 97.20.Wt, 97.60.Bw, 98.38.Mz

INTRODUCTION

Dust grains in the early universe have great impacts on the evolutional history of the universe: Dust grains control the energy balance in interstellar space through absorption of stellar light and re-emission of it, and play critical roles in the formation processes of stars and galaxies. In particular, their thermal emission greatly increases the efficiency of cooling of gas in metal-poor circumstances, which causes the star-forming gas cloud to fragment into low-mass gas clumps of 0.1–1 $M_\odot$ for metallicity of 10^{-6} to 10^{-5} $Z_\odot$ [1, 2, 3]. The absorption and thermal emission by dust grains heavily depend on their composition, size, and amount. Thus, it is one of the most important subjects in astrophysics to elucidate the origin and evolution of dust grains.

The dominant sources of dust in the early universe are considered to be supernovae (SNe) evolving from the early generations of massive stars. Theoretical studies have investigated the formation of dust in primordial Type II SNe (SNe II) [4, 5] and pair-instability SNe [5, 6], and have revealed the composition, size, and mass of dust formed in the ejecta; for SNe II, dust grains of 0.1–2 $M_\odot$ are formed, which is in good agreement with the amount required to account for dust content in high-redshift galaxies [7, 8]. However, the reverse shock induced by the interaction of the SN ejecta with the surrounding medium reprocesses the newly condensed dust grains and makes their size and mass significantly different from those at the time of dust formation [9, 10].

In this proceedings, we present the calculations for the processing of dust through the collisions with the reverse shocks and its transport within Population III SN remnants (SNRs), in order to reveal the size and amount of dust injected from SNe into the interstellar medium (ISM). The results of calculations show that a part of the surviving dust grains are accumulated in the dense SN shell. These piled-up grains may have significant influences on the elemental abundances of the second-generation stars formed there. Therefore, assuming that the composition of the piled-up grains reflects the elemental composition of those stars, we explore the abundance patterns of the stars formed in the dense shell of Population III SNRs and compare to those observed in hyper-metal-poor (HMP) and ultra-metal-poor (UMP) stars.

EVOLUTION OF DUST IN PRIMORDIAL SNRS

The calculations of the dust evolution in SNRs are described in detail by Nozawa et al. (2007) [10]. By taking the size distribution and spatial distribution of each dust species from the dust formation model by [5] as the initial conditions, the transport of dust and its destruction by sputtering are calculated. The time evolution of the gas temperature and density in SNRs expanding into the uniform ISM with the hydrogen number density of $n_{\rm H,0} = 0.1$, 1, and 10 cm^{-3} are calculated by adopting the hydrodynamic models of Population III SNe by [11]. In what follows, we present the results for the evolution of the dust formed in the unmixed ejecta of SNe II with the progenitor masses of $M_{\rm pr} = 13$, 20, 25, and 30 $M_\odot$ and explosion energy of 10^{51} ergs.

In Figure 1*a*, we show the time evolutions of positions of C, Mg_2SiO_4, and Fe grains within the SNR for $M_{\rm pr} = 20\ M_\odot$ and $n_{\rm H,0} = 1$ cm^{-3}, and the time evolutions of their radii are given in Fig 1*b*. The thick solid lines in Fig. 1*a* depict the positions of the forward shock, the reverse shock, and the surface of the He core. C, Mg_2SiO_4, and Fe grains comove with the gas until they encounter the reverse shock at 3650 yr, 6300 yr, and 13000 yr, respectively. Once dust grains intrude into the reverse shock, their fates strongly depend on their initial radii $a_{\rm ini}$ and compositions. Because the deceleration rate of a grain is inversely proportional to its radius, the relatively small grains with $a_{\rm ini} = 0.01\ \mu$m (*dotted lines*) are efficiently decelerated by the gas drag and are trapped in the hot gas of $\geq 10^6$ K created by the passage of the reverse and forward shocks. These small grains captured in the hot gas are completely destroyed by the thermal sputtering. C, Mg_2SiO_4, and Fe grains with $a_{\rm ini} = 0.1\ \mu$m (*dashed lines*) penetrating into the hot gas are eroded due to the kinetic and/or thermal sputterings, and their radii are reduced by 43%, 69%, and 52%, respectively. C and Mg_2SiO_4 grains of $a_{\rm ini} = 0.1\ \mu$m are finally

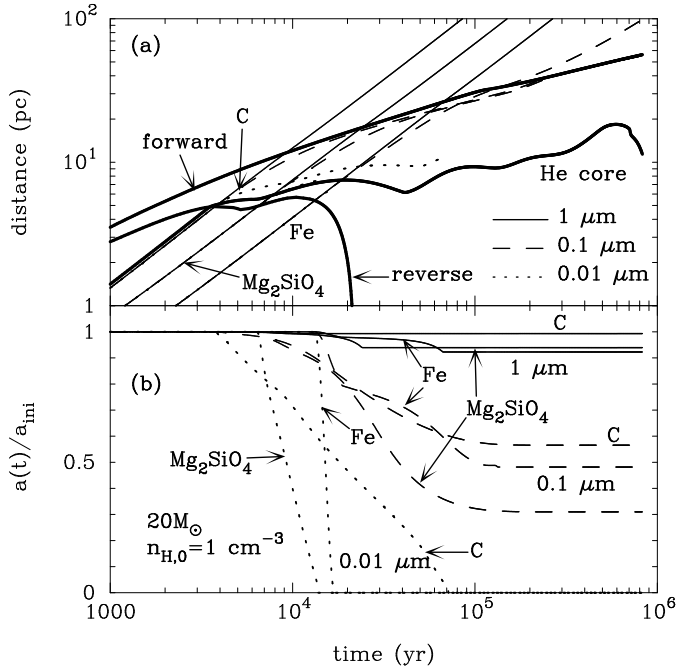

FIGURE 1. Time evolutions of (*a*) positions of C, Mg_2SiO_4, and Fe grains within the SNR for $M_{\rm pr} = 20$ $M_\odot$ and $n_{\rm H,0} = 1$ cm^{-3} and (*b*) ratios of their radii to the initial ones. The evolution of dust with $a_{\rm ini} =$ 0.01, 0.1, and 1 μm is denoted by the dotted, dashed, and solid lines, respectively. In (*a*), the positions of the forward shock, the reverse shocks, and the surface of the He core are indicated by the thick solid lines.

trapped in the dense SN shell formed at $\sim 2\times 10^5$ yr, where the dust grains are no longer eroded by the thermal sputtering because the gas temperature drops down quickly below 10^5 K [12]. The 0.1 μm-sized Fe grains with higher bulk density are ejected into the ISM. Since the deceleration by the gas drag is inefficient, grains with $a_{\rm ini} = 1$ μm (*solid lines*) also go across the outwardly expanding shock front and are injected into the ISM without being processed significantly,

The behaviors of the transport and destruction of dust in a SNR heavily depend on the density of gas in the ISM; as the ISM gas density is higher, the density of the shocked gas is higher, which leads to the efficient deceleration and erosion of dust through more frequent collisions with the hot gas. As a result, the lower limit of the initial radius of dust injected into the ISM increases with increasing the ISM density and is 0.03, 0.2, and 0.5 μm for $n_{\rm H,0} = 0.1$, 1, and 10 cm^{-3}, respectively. Furthermore, the initial radius below which dust is completely destroyed is enhanced by the increase of the density in the ISM, and is 0.01, 0.05, and 0.2 μm for $n_{\rm H,0} = 0.1$, 1, and 10 cm^{-3}. Accordingly, as shown in Figure 2, the total mass of the surviving dust decreases with increasing the ambient density and spans the range of 0.01–0.8 $M_\odot$ for $n_{\rm H,0} = 10$ to 0.1 cm^{-3}, depending on the progenitor mass. In any cases, the resulting size distribution of the dust that survives the destruction shows a serious lack of small-sized grains, in comparison with that at the time of dust formation. Note that the evolution of dust within a SNR does not depend on the progenitor mass considered here because the same explosion energy results in the similar time evolution of the gas temperature and density.

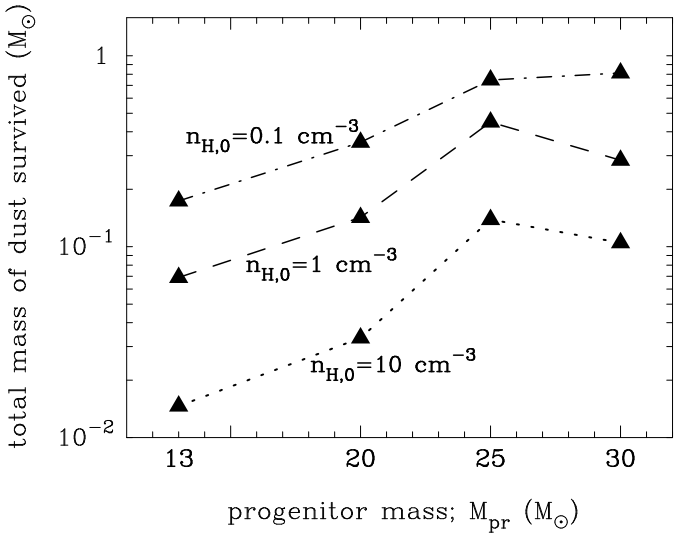

FIGURE 2. Total mass of surviving dust vs. the progenitor mass. The results for $n_{\rm H,0} = 0.1$, 1, and 10 cm^{-3} are connected by the dot-dashed, dashed, and dotted lines, respectively.

ELEMENTAL ABUNDANCES IN THE DENSE SN SHELL

Currently known most iron-deficient stars, HE 0107-5240 with [Fe/H] $= -5.3$ ([13, 14]) and HE 1327-2326 with [Fe/H] $= -5.45$ ([15, 16]) show peculiar abundance patterns: more than 100 times excesses of C, N, and O and 1–100 times enhancements of Mg and Si relative to Fe. Also, UMP star, HE 0557-4880 with [Fe/H] $= -4.75$ ([17]) exhibits a large ($\sim$50 times) overabundance of C. Although the elemental compositions of these low-mass stars are expected to reflect the nucleosynthesis in the very early generations of stars, the origin of the abundance patterns in HMP and UMP stars is still an open question.

The results for the evolution of dust within a SNR presented in this paper show that the dust grains which are not injected into the ISM but survive the destruction through the collision with the reverse shock are accumulated in the dense SN shell in 10^5–10^6 yr. This transport of dust to the SN shell may not only enable the formation of stars with solar mass scales there [1, 2, 3] but also influence the elemental abundance of those stars. Therefore, based on the composition of the piled-up grains, we investigate the metal abundance patterns of the stars formed in the dense shell of SNRs and compare to those observed in HMP and UMP stars, assuming that they are the second-generation stars formed in the shell of Population III SNRs.

The results for the elemental composition and metallicity in the dense shell are summarized in Table 1 for various progenitor masses and ambient densities. Metallicity in the shell is in the range from 10^{-6} up to 10^{-4} $Z_\odot$, which is high enough to form low-mass stars with 0.1–1 $M_\odot$ [1, 2, 3]. We can also see that most of calculated [Fe/H] spans the range of -6 to -4.5, which are in good agreement with those for HMP and UMP stars.

In Figure 3*a*, we show the abundances of Mg and Si (*upper panel*) and C and O

TABLE 1. Elemental composition and metallicity in the dense shell of primordial SNe II for various progenitor masses and ambient densities.

$M_{\rm pr}$ ($M_\odot$)	[Fe/H]	[C/Fe]	[O/Fe]	[Mg/Fe]	[Si/Fe]	[Al/Fe]	[S/Fe]	$\log(Z/Z_\odot)$
$n_{\rm H,0} = 0.1$ cm^{-3}								
13	−6.43	−0.274	−0.699	−0.230	1.92	−2.60	0.239	−5.89
20	−5.20	0.117	−0.595	0.034	0.410	−1.97	0.242	−5.44
25	−5.90	1.11	−1.42	−0.500	−0.552	−0.563	0.242	−5.55
30	−5.56	0.566	−0.043	0.739	0.866	0.905	0.242	−5.33
$n_{\rm H,0} = 1$ cm^{-3}								
13	−5.15	1.11	−0.555	−0.459	1.01	–	−2.18	−4.72
20	−5.53	0.992	0.585	1.16	1.87	–	0.200	−4.68
25	−5.23	1.09	−0.412	0.407	0.989	–	0.241	−4.79
30	−5.11	0.797	0.242	1.09	1.26	−5.72	0.242	−4.60
$n_{\rm H,0} = 10$ cm^{-3}								
13	−4.13	0.284	−2.54	−3.89	0.599	–	–	−4.40
20	−4.92	0.946	−2.15	−1.80	2.14	–	–	−4.09
25	−5.10	1.60	0.122	0.232	2.34	–	−1.45	−3.91
30	−5.11	−0.207	0.375	−1.23	2.66	–	−0.696	−3.84

(*lower panel*) in the dense shell as a function of [Fe/H] for the ISM density of 1 cm^{-3}. The results of calculations are drawn by the filled symbols, and the observational data of HMP and UMP stars are plotted by the open symbols. We can see that in addition to Fe, the calculated abundances of Mg and Si can also reproduce the observations of HMP stars with 1–100 times overabundances seen in HMP stars. Some models (such as $M_{\rm pr} =$ 20 and 30 $M_\odot$ for $n_{\rm H,0} = 0.1$ cm^{-3}) also show the modest overabundances for both Mg and Si (see Table 1). Because the elemental composition of dust piled up in the shell can reproduce the abundance patterns of refractory elements such as Mg, Si, and Fe in HMP and UMP stars, we can conclude that the transport of dust separated from metal-rich gas within SNRs can be responsible for the abundance patterns in HMP and UMP stars, if they are the second-generation stars formed in the dense shell of primordial SNRs. However, more than one hundred times excesses of C and O observed in HMP and UMP stars cannot be reproduced by any models considered here.

The reasons is that in the calculation we assumed that the metal-rich gas in the ejecta of SN does not mix with the gas in the shell. Then, as an extreme case, we examine the abundance patterns in the shell by considering that in addition to the piled-up grains, the gas outside the innermost Fe layer of the SN is incorporated into the shell. The results are shown by the filled symbols in Figure 3*b*. This case can produce the extreme overabundances ($\sim$1000 times) of C and O, but results in unreasonable excesses ($\geq$100 times) of Mg and Si, which is not in agreement with the observations. Nevertheless, it might be possible to reproduce the elemental abundances of HMP stars if the Si-Mg-rich layer is not mixed with the gas in the shell. Anyway, it is necessary to examine what extent of the gas in the SN ejecta can mix with the gas in the shell when the second-generation stars form in the SN shell. In the future works, we will consider this subject.

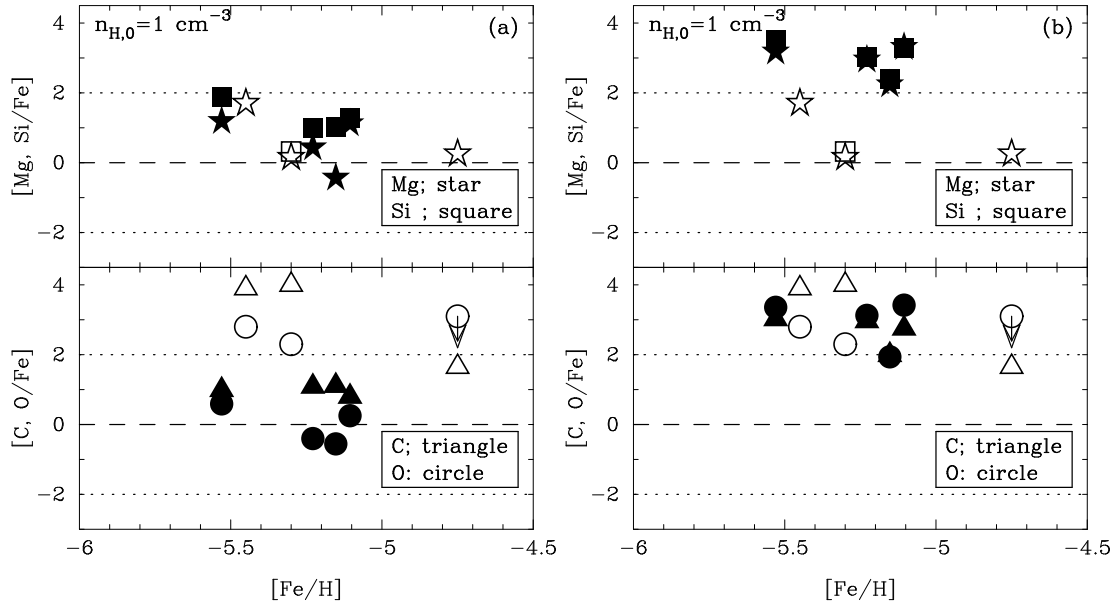

FIGURE 3. Abundances of Mg and Si (*upper panel*) and C and O (*lower panel*) in the shell of the SNR for $n_{\rm H,0} = 1$ cm^{-3}; (*a*) the elemental abundances obtained from the grains piled up in the shell, and (*b*) the elemental abundances including the gas outside the innermost Fe layer as well as the piled-up grains. The results of calculations are shown by the filled symbols. The observational data for HMP and UMP stars are denoted by the open symbols and are taken from [14, 15, 16, 17, 18].

ACKNOWLEDGMENTS

This work has been supported in part by a Grant-in-Aid for Scientific Research from the Japan Society for the Promotion of Sciences (19740094, 18104003).

REFERENCES

1. Omukai, K., et al., *ApJ*, **626**, 627–643 (2005)
2. Tsuribe, T., & Omukai, K., *ApJ*, **642**, L61–L64 (2006)
3. Schneider, R., et al., *MNRAS*, **369**, 1437–1444 (2006)
4. Todini, P., & Ferrara, A., *MNRAS*, **325**, 726–736 (2001)
5. Nozawa, T., et al., *ApJ*, **598**, 785–803 (2003)
6. Schneider, R., Ferrara, A., & Salvaterra, R., *MNRAS*, **351**, 1379–1386 (2004)
7. Morgan, H. L., & Edmunds, M. G., *MNRAS*, **343**, 427–442 (2003)
8. Dwek, E., Galliano, F., & Jones, A. P., *ApJ*, **662**, 927–939 (2007)
9. Bianchi, S., & Schneider, R., *MNRAS*, **378**, 973–982 (2007)
10. Nozawa, T., et al., *ApJ*, **666**, 955–966 (2007)
11. Umeda, H., & Nomoto, K., *ApJ*, **565**, 385–404 (2002)
12. Nozawa, T., Kozasa, T., & Habe, A., *ApJ*, **648**, 435–451 (2006)
13. Christlieb, N., et al., *Nature*, **419**, 904–906 (2002)
14. Christlieb, N., et al., *ApJ*, **603**, 708–728 (2004)
15. Frebel, A., et al., *Nature*, **434**, 871–873 (2005)
16. Aoki, W., et al., *ApJ*, **639**, 897–917 (2006)
17. Norris, J. E., et al., *ApJ*, **670**, 774–788 (2007)
18. Frebel, A., et al., *ApJ*, **638**, L17–L20 (2006)